Spatio-temporal constraints on magma storage and ascent conditions in a transtensional tectonic setting: The case of the Terceira Island (Azores)

Revision 2

Vittorio Zanon [1]* and Adriano Pimentel [2,1]

[1] Centro de Vulcanologia e Avaliação de Riscos Geológicos, Rua Mãe de Deus, 9501-801 Ponta Delgada, Portugal

[2] Centro de Informação e Vigilância Sismovulcânica dos Açores, Rua Mãe de Deus, 9501-801 Ponta Delgada, Portugal

** Corresponding author*

Keywords

Magma ponding, Fissure zones, Fluid inclusions, Re-equilibration, Olivine, Azores

Abstract

The mafic magmatism of the last 50 ka on Terceira Island, Azores archipelago, occurred along three segments of the fissure zone that crosses the island. The two subaerial segments developed with different trends over pre-existing, quiescent or extinct, central volcanoes. The Serreta submarine ridge is the offshore segment of the fissure zone which erupted recently in AD 1998-2001. The combined study of CO_2+H_2O fluid inclusions hosted in mafic minerals and rock geochemistry of the magmas, reveals different storage and ascent conditions among the fissure zone segments. The maximum pressure of fluid trapping for all the fissure systems occurred at the Moho Transition Zone, between 498 MPa and 575 MPa (20.3-21 km deep). At this depth interval all magmas stagnated for some time, before ascending towards the surface, experiencing fractional crystallization and degassing. Magmas of the southeastern and Serreta segments of the fissure zone ascended rapidly through the crust without further stops. Those of the central segment experienced a multi-step ascent, with fluid trapping at 406 MPa and 209 MPa (16.5-8.5 km deep) and associated geochemical evolution towards trachybasalt.

The magma ascent below the different segments of the fissure zone varies from almost isochoric at the submarine segment, associated with minimum re-equilibration of the inclusions, to polybaric slow ascent at the central segment, associated to almost complete re-equilibration of the inclusions. Variable degrees of re-equilibration and multi-step ascent may be linked to both the presence of pre-existing intracrustal crystallized bodies of more evolved composition and the stress field acting on this area. The latter responds to the local and shallow conditions related to the presence of older central volcanoes and to the main regional spreading direction of the Terceira Rift, which at regional scale, is approximatively orthogonal to the fissure zone axis.

INTRODUCTION

The location and structure of magma storage systems, the amount of melt available for mobilization prior to eruption, and its path and rate of ascent are all fundamental information to achieve a better understanding of the behavior of volcanic systems. These elements are known in well-monitored and frequently erupting basaltic volcanoes, such as Etna, Stromboli, Kilauea and Piton de la Fournaise, and fairly understood in those with higher associated risk but more infrequent activity (e.g. Vesuvius, La Peleé, the Cascades volcanoes). However, aside from the abovementioned cases, such information is completely unknown for many oceanic islands, such as the Azores.

The Azores islands are volcanic systems predominantly formed by basaltic fissure zones, where magma, collected at the Moho Transition Zone, is mobilized in response to tectonic stress (Haase and Beier 2003; Zanon et al. 2013; Zanon and Frezzotti 2013). Typically, eruptive fissures open in the same area during a limited period (a few thousands of years) before migrating to another area nearby (Hildenbrand et al. 2008). Erupted lavas are poorly evolved basalts (e.g. Beier et al. 2007; 2008; 2012), which ascend from the mantle due to extensional tectonics. The interaction of extensional fissures with transtensional faults determines the formation of short-lived and shallow-level magma reservoirs, leading to the establishment of centralized feeding conduits or a series of closely-spaced feeder dykes, and, progressively, to the development of larger volcanic systems (Miranda et al. 1998).

On the Azorean island of Terceira eruptions occur at both central volcanoes and various segments of a fissure zone that crosses the island and extends offshore. Magmas from central volcanoes are generally highly differentiated (mugearites-trachytes and peralkaline rhyolites), while those from the fissure zone consist of basalt-trachybasalt associations (Self and Gunn

1976; Mungall and Martin 1995; Madureira et al. 2011). The mafic magmas erupted in the last 50 ka were emitted from different segments of the fissure zone and are characterized by a variable degree of evolution. The subaerial fissure system is located between closely-spaced central volcanoes of different age.

Possibly, the presence at depth of partially crystallized bodies of evolved composition, related to the central volcanoes, influenced the magma ascent at the fissure zone segments of the island, promoting the formation of intracrustal storage areas and enhancing their chemical evolution through fractional crystallization. This hypothesis is here investigated through the microthermometric study of fluid inclusions trapped in mafic minerals found in the magmas from the different segments of the fissure zone. The data of samples from the two subaerial segments and the submarine segment are compared also in terms of geochemical characteristics of the magmas. This method is a rapid and reliable way to constrain the spatial and temporal evolution of the magma storage areas at crustal depths. In fact, the same methodology has been successfully applied to various volcanic systems, including the Aeolian (Zanon et al. 2003; Bonelli et al. 2004; Zanon and Nikogosian 2004; Di Martino et al. 2010) and Canary islands (Hansteen et al. 1991; Klügel et al. 1997; Hansteen et al. 1998; Klügel et al. 2005; Galipp et al. 2006; Stroncik et al. 2009). More recently, it has been also applied to the islands of Pico and Faial, also in Azores (Zanon and Frezzotti 2013), where basalts are mobilized by extensional tectonics and ascend from the ponding area located at the Moho Transition Zone, without further stops in the crust.

GEOLOGICAL SETTING

Terceira Island is located in the central-north Atlantic Ocean, near the triple junction among the North American, Eurasian and Nubian plates. This area of the Atlantic is characterized by a complex geodynamic setting with the presence of the Mid-Atlantic Ridge to the west and the Gloria strike-slip fault to the east (Fig. 1a). A regional WNW-ESE trending system (the so called Terceira Rift), characterized by a slow and asymmetric spreading rate from northeast to the southwest (e.g. Marques et al. 2013), is located between the two abovementioned structures.

Terceira is formed by two extinct and two quiescent central volcanoes and a diffuse fissure zone (Fig. 1b). Ages of all eruption products show an overall east to west younging progression, although with contemporaneous periods of activity (Calvert et al. 2006 and references therein). Cinco Picos and Guilherme Moniz are the two oldest and extinct volcanoes (>388 ka and >270 ka, respectively; Calvert et al., 2006), located in the eastern and central part of the island. The calderas are filled by more recent lavas erupted from the fissure zone. Pico Alto Volcano is older than 141 ka (Gertisser et al. 2010) and is located north of Guilherme Moniz, while the western third of the Terceira is formed by the well-preserved conical-shaped volcano of Santa Bárbara, the age of which is unknown.

The fissure zone crosses the island along a general WNW-ESE direction and extends offshore, forming submarine ridges. Its presence is marked by alignments of scoria and spatter cones and fissures which erupted basaltic (sensu lato) lavas. In comparison with fissure systems present on other islands of the archipelago, these alignments are made up of fewer cones, suggesting a lower number of eruptive events. A careful observation of the Digital Elevation Model (DEM) in Figure 1 reveals that the fissure zone is segmented. The overall WNW-ESE direction is interrupted in the area of Cinco Picos and Guilherme Moniz calderas, where the possible effect of NW-SE tectonics has exerted a clockwise rotation of the eruptive axis.

The age of the fissure zone is currently constrained between late Pleistocene (>43 ka; Calvert et al. 2006) and the present, although some activity may be older. The eruptive vents show a general progressive younger age from southeast to northwest, with historical eruptions inland (AD 1761) and offshore in the Serreta submarine ridge (AD 1867 and AD 1998-2001; Fig. 1b).

The tectonics of the island responds to the dynamics of the WNW-ESE trending Terceira Rift, as most structural features are sub-parallel to this regional direction (Fig. 1b; Self 1976; Tzanis and Makropoulos 1999; Quartau et al. 2014). The main feature is the NW-SE oriented Lajes graben in the northeast sector of the island. Other WNW-ESE to NW-SE trends including volcano-tectonic alignments of vents and faults provide evidence of a transtensive regime on the island.

METHODS

For this study we selected porphyritic lava samples emitted from the fissure zone segments across the island and offshore. Rocks containing olivine and clinopyroxene were chosen for the study of fluid inclusions, as this mineralogy is representative of the early stages of evolution of magmas.

Whole-rock analyses were performed by Activation Laboratories (Canada). Alkaline dissolution with lithium metaborate/tetraborate followed by nitric acid was used on 1 gram of rock powder before being fused in an induction furnace. The melt was then poured into a solution of 5% nitric acid containing cadmium as an internal standard and continuously stirred until complete dissolution was achieved (~30 minutes). The samples were contemporaneously analyzed by a Perkin Elmer 9000 inductively coupled plasma mass spectrometer (ICP-MS) and an Agilent 735 inductively coupled plasma atomic emission spectrometer (ICP-AES). Analytical precision (2σ) was better than 5% for most major elements and 10% for most minor and trace elements. Nine international rock standards were used to calibrate the two methods. Whole-rock and mineral chemistry are reported in the supplementary material.

A JEOL JXA 8200 Superprobe, equipped with five wavelength-dispersive spectrometers, energy-dispersive spectrometer and cathodoluminescence detectors (Dipartimento di Scienze della Terra, "Ardito Desio" University of Milan, Italy) was used to analyze mafic crystalline phases and glasses. A spot size of 1 μm with a beam current of 15 nA was used for the mineral phases, whereas a spot size of 5-7 μm, according to the available surface to be analyzed, and a beam current of 2 nA were applied to glasses. Count times were 30 s on the peak and 10 s on each background. Natural and synthetic minerals and glasses, used as standards, were used for calibration within 2% at 2σ standard deviation. Raw data were corrected applying a Phi-Rho-Z quantitative analysis program. The typical detection limit for each element is 0.01%.

Geobarometric data were obtained by microthermometry of the fluid inclusions contained in mafic phenocrysts. About 250/300 olivines and 100/150 clinopyroxenes up to 500 μm in size were handpicked from crushed rock, cleaned with deionized water, embedded in acetone-soluble epoxy and doubly polished up a final thickness of 120-80 μm.

Microthermometry of fluid inclusions were carried out on a Linkam MDSG600 heating-cooling stage, calibrated using synthetic H_2O-CO_2 inclusions (triple point for CO_2 and H_2O at -56.6 °C and 0 °C, respectively). Melting and homogenization temperatures are reproducible to ±0.1 °C. For all the runs, the heating rate was in the range 0.2–0.5 °C/min. The equation of Span and Wagner (1996) was used to calculate density values of pure CO_2 fluid. These values were then corrected for the probable presence of 10 mole% of H_2O, following the method suggested in Hansteen and Klügel (2008). Finally, isochores for H_2O-CO_2 fluids were derived using the model of Sterner and Bodnar (1991) by means of the computer program FLUIDS (Bakker, 2003). Despite the fact that the model is experimentally calibrated up to 700 °C and 600 MPa, its application to higher temperatures provided a good fit. Final pressure calculations were obtained from the intersection of isochores with the maximum temperature of crystallization inferred from olivine thermometers (Putirka 2008; Beattie 1993; Shejwalkar and Coogan 2013).

Finally, direct density measurements were carried out on some samples with a resolution of 1 $kg \cdot m^{-3}$, using a MD 200s electronic densimeter and corrected for porosity.

SAMPLE DESCRIPTION

The studied samples are lavas erupted from the different segments of the fissure zone between less than 50 ka and AD 2001 (Fig. 2). The main petrographic characteristics of these samples are summarized in Table 1. In contrast to lavas from Pico, Faial and São Miguel islands (Zanon et al. 2013; Zanon and Frezzotti, 2013; Zanon 2014), the samples are almost aphyric (Fig. 3a) to poorly porphyritic, with a maximum phenocrysts content of ~22 vol% (Fig. 3b) and rare occurrences of megacrysts of olivines in only a few samples. The mineral assemblage consists of phenocrysts of olivine, clinopyroxene, plagioclase ±oxides in variable proportions. Common textures are intersertal and intergranular, with a few glomeroporphyritic aggregates, while only in the lava balloons, from the AD 1998-2001 Serreta submarine eruption, textures range from vitrophyric with cryptocrystals to intersertal due to the extent of seawater quenching.

Olivine phenocrysts up to 2 mm in size are present in some samples in variable amounts (≤13 vol%). They are euhedral or subhedral, or rarely skeletal, and the core Mg number [Mg# = 100·Mg/(Mg+Fe)] ranges from 80 to 90%. Fluid inclusions are present in ~2-4% of these crystals. This percentage increases to 8% only in the olivines from the lava balloons. Microphenocrysts <0.5 mm in size (Fig. 3b) are much more abundant and present in all samples, but are devoid of fluid inclusions.

Clinopyroxene phenocrysts are typically ≤1 vol% in most samples, with augite and augitic diopside composition (Wo_{33-38}, En_{38-48}, Fs_{3-11}). They are <5 mm in size, euhedral and zoned, with rare evidences of disequilibrium (i.e. embayments and reaction rims). Their core Mg number [$Mg\# = 100 \cdot Mg/(Mg+Fe^{+2}+Fe^{+3}+Mn)$] varies from 81-86% in the subaerial lavas and from 71-76 in the lava balloons. Only rare crystals contain fluid inclusions. Microphenocrysts (~1.5 mm in size) are more abundant but devoid of fluid inclusions.

Plagioclase phenocrysts up to 5 mm in size are rare (≤4 vol%) and are characterized by euhedral, either tabular or acicular morphology and oscillatory or reverse zoning. Their composition varies from andesine to labradorite (An_{63-72}). Rare anhedral crystals with signs of disequilibrium (sieve texture) and bytownitic composition (An80) have also been found. No fluid inclusions have been found here. Plagioclase microphenocrysts (<0.5 mm) are abundant in many samples.

Finally, rare titanomagnetites are present as phenocysts (≤0.2 vol%) in few samples, while are common in all samples as microphencrysts. Apatite and ilmenite are sometimes present in the groundmass.

ROCK GEOCHEMISTRY

The studied compositions are transitional to mildly alkaline basalts and trachybasalts (Fig. 4a) with MgO content ranging from 4.5 to 11.6 wt%. The lowest MgO value characterizes a lava of the central segment of the fissure zone (Cfz), while the highest derives from a more porphyritic rock of the southeastern segment (SEfz). With the exception of three samples which are mildly silica-undersaturated (ne ≤2.14%), the others are silica-saturated, with up to 8.7% normative hyperstene (Table 2).

All major elements, except CaO, show a general increase with decreasing MgO, however data are scattered and not linearly correlated. Samples from the Cfz have lower MgO content (≤6.5 wt%) and show, on average, higher Na_2O, K_2O, P_2O_5 and TiO_2 contents than the corresponding rocks from the SEfz. The variations of compatible trace elements such as Ni, Sc, Cr, Cu and Co are positively correlated with MgO, whereas Large Ion Lithophile Elements (LILE: Rb, Ba, K, Cs) and High Field Strength Elements (HFSE: Ta, Nb, Zr, Hf, Th, U) have opposite trends.

All trace element patterns are quite similar, with marked K and Pb negative spikes and limited Th, U, Hf and Zr fractionation (Fig. 4b). The rocks from the Cfz, which are the most evolved, are consequently the most enriched in incompatible elements when compared to the composition of the primordial mantle (McDonough and Sun, 1995). All patterns of Rare Earth Elements (REE) are smooth and slightly enriched in lighter elements and without the Eu anomaly (Fig. 4c).

The variations of the ratio CaO/Al_2O_3, correlated to those of FeO_t/MgO, and the positive correlation between the variations of compatible trace elements and MgO qualitatively would suggest that all these compositions are related to each other by a process of fractional crystallization, involving the removal of stable proportions of mafic phases from a common and more primitive parental magma (Fig. 5a). However, LILE and U and Th are incompatible within the structures of both clinopyroxene and olivine, therefore, during the fractional crystallization of these phases ratios among these elements in the parental liquid cannot change. In our compositions these ratios are very scattered (Fig. 5b). Similar conclusions are derived from the analysis of the variation among light and heavy REE. These elements are generally incompatible in both olivine and clinopyroxene, although they have variable partition coefficients. Variations in the ratios of these elements are too large for a process of removal of mafic phases (Fig. 5c). Finally, the variable degree of silica saturation is not related to the Mg# of the rocks. All these elements indicate that the characteristic geochemical signature of each of these samples reflects variations of the degree of melting at the source or the extent of high pressure fractional crystallization from a pristine liquid. Therefore, each of these compositions does not result from the evolution of a common parental melt in a large magma reservoir at shallow-to-intermediate depth, but rather represents a different melt, which behaved as a single magma batch.

PETROGRAPHY AND MICROTHERMOMETRY OF FLUID INCLUSIONS

In general, the occurrence of fluid inclusions in Terceira lavas is rare (Table 2); a small number of inclusions are present in ~2% of olivine phenocrysts and in ~0.5% of clinopyroxene of the lavas from the subaerial segments of the fissure zone. In the lava balloons from the Serreta submarine fissure zone (SERfz), a larger number of inclusions are present in ~10% of olivines and ~2% of clinopyroxenes. No inclusions have been found in the rare megacrysts and in microphenocrysts.

Textural characteristics of fluid inclusions allow us to distinguish two types of populations. Type-I inclusions are well rounded, either isolated or clustered, up to 25-35 μm in size and randomly located at the core of phenocrysts. In some cases they are present together with small crystalline phases and silicate melt inclusions between growth zones of the phenocrysts. The inclusions do not contain crystal phases. These textural characteristics indicate that these inclusions are trapped during the early stages of crystallization of the phenocrysts. Many inclusions show evidence of density partial re-equilibration i.e., micro-cracks departing from the main cavity and/or a halo of minute inclusions, around the main cavity, and/or a dark aspect (Viti and Frezzotti 2000; Viti and Frezzotti 2001).

Type-II fluid inclusions are more abundant in the mafic phases of the lava balloons, when compared to the subaerial samples. They commonly occur as trails of variable length and thickness, which lined completely healed fractures, limited by grain boundaries. Inclusions are typically <10 μm, usually rounded and may coexist with both Type-I (Fig. 3c) and silicate melt inclusions with variable size and degree of crystallization. These inclusions formed during episodes of deformation/cracking of the host crystals after their growth.

Frozen inclusions melt instantaneously within a temperature interval between 57.3 and 56.4 °C, with most of the data at 56.7 °C. These temperatures suggest that trapped fluids are composed of almost pure CO_2 together with the presence of few moles (less than 1%; Van den Kerkhof 1990) of other volatile species (i.e. N_2 and SO_2). This small amount does not significantly affect the interpretation of entrapment conditions (Van den Kerkhof 1990; Frezzotti et al. 2002), and for this reason these inclusions can be treated as composed of pure CO_2. Clathrates are not detected but liquid H_2O was rarely optically observed in some large Type-I inclusions in olivines. According to Lamadrid et al. (2014), H_2O in small size inclusions is not detectable either optically or by Raman spectroscopy, as it forms a very thin film at the walls of the inclusion. Final homogenization occurs into the liquid (Th_L). Only a single inclusion homogenizes into the vapor phase (Th_V).

Type-I fluid inclusions in the olivines from the subaerial lavas have values of Th_L from 23.5 °C to 31 °C (480-730 kg·m^{-3}) and those in the clinopyroxenes from 30.6 °C to 31 °C (480-560 kg·m-3). Inclusions inside the olivines of the lava balloons have values of Th_L from 18.8 °C to 26.1 °C (690-790 kg·m^{-3}).

Type-II fluid inclusions in the olivines from the subaerial lavas have values of Th_L from 24.3 °C to 31 °C (480-720 kg·m^{-3}). A single inclusion homogenized into the vapor phase at 31 °C (460 kg·m^{-3}). Inclusions in the olivines from the lava balloons have values of Th_L from 23.7 °C to 30.2 °C (580-730 kg·m^{-3}), while in clinopyroxenes from 27.2 °C to 31 °C (470-670 kg·m^{-3}). The frequency-distribution histograms of Th_L of fluid inclusions in olivines and clinopyroxenes (Fig. 6a, b, c) is built by merging the data from lavas belonging to the same segment of the fissure zone. These plots show polymodal distribution of data. The same characteristics can be observed in histograms of density data distribution (Fig. 6d, e, f).

MAGMA PONDING AND ASCENT CONDITIONS

Barometric constraints from fluid inclusions

After formation, a crystal may stretch or even crack, as a function of the strain rate, due to the variations of confining pressure and temperature. As result, trapped inclusions re-equilibrate to variable extents, changing their original density values. As an extreme case, new cracks form around the main inclusion cavity, allowing the fluid to redistribute into them, which results in an inclusion larger than the original. These processes are common in a magmatic assemblage during the ascent history of the carrier magma (Bodnar 2003). For this reason, all inclusions suffered at least a minimum degree of re-equilibration, although some features are too small to be resolved by optical microscopy, and require the use of transmission electron microscopy (Viti and Frezzotti 2000; Viti and Frezzotti 2001). The smallest inclusions have the highest chance to have suffered minimum degrees of re-equilibration (Fig. 7) and we assume that those inclusions, without visible re-equilibration features, are the most adequate to provide information on the depth of the magma reservoir (Andersen and Neumann 2001). A latter event of fluid trapping will produce a second mode in a fluid density distribution histogram. Also in this case, the densest inclusion of this population reveals information useful to locate the magma reservoir.

The composition of trapped fluids is mostly CO_2 and few moles of other volatile species. However, H_2O, as main component of exolved fluid, is expected to be originally present inside inclusions, and indeed it was directly observed at the microscope, in some rare inclusions. Either hydrogen diffused at high temperatures into the host olivine (Gaetani et al. 2012) or it probably reacted with the host mineral at low temperatures, forming hydrous carbonates (Andersen and Neumann 2001; Frezzotti et al. 2002). For these reasons, according to Dixon and Stolper (1995), Dixon (1997) and Hansteen and Klügel (2008) and here corroborated by direct observation of the presence of H_2O in fluid inclusions, we hypothesized an original fluid composition at the time of trapping of χ_{H2O}=0.1 and χ_{CO2}=0.9.

In order to obtain barometric information on the magma plumbing system, it is necessary to calculate the magmatic temperature at the moment of fluid trapping. We applied thermometers based upon the equilibrium of olivine-liquid to the groundmass glass to have a first order estimation of the eruptive temperature. Only two microlitic olivines from a lava balloon ($Fo_{78\text{-}80}$) were found to be in equilibrium and provided a temperature of 1139 °C and 1146 °C (±30 °C) using the thermometer of Putirka (2008). The thermometer of Beattie (1993) yielded 1154 ±10 °C. The calculation of the olivine crystallization temperature requires the compositions of melt inclusions and of their hosts, but the composition published in Kueppers et al. (2012) for the AD 1998-2001 submarine eruption did not equilibrate, due to post-entrapment crystallization. For this reason, we have applied a chemical thermometer based upon the Ca content in olivine (Shejwalkar and Coogan 2013), despite our olivine compositions are off the field of application. However, we hypothesized that the real conditions of crystallization of the olivines in this study were not too far from those required by this thermometer. The resulting temperatures are shown in Figure 8. Despite a minimum scattering of the data, many values peak at 1170 °C, which is only about 25-30°C higher than the eruptive temperature and 20 °C higher than the calculated for Pico and Faial islands (Zanon and Frezzotti 2013). However, the determination of a very precise temperature is not a critical element for the validation of the barometric data of fluid inclusions (Roedder 1965; 1983); in fact a difference in this temperature of ±20 °C changes the resulting values of pressure only by ±8 MPa (1.5%).

The pressure conditions for magma storage were obtained from isochores distribution at 1170 °C (Fig. 9). The error associated to this calculation is ±1 MPa. The possibility that the trapped fluids preserve their original density depends on the strength of the crystal to external stresses, on the P-T path during magma ascent. The effect of re-equilibration on the fluids trapped in the mafic phases from lava compositions of the three segments of the fissure zone is shown in the pressure scheme of Figure 10. The highest lithostatic pressure conditions are recorded by fluids in the olivines of the lava balloons from the SERfz (575 MPa). Differently, inclusions hosted in clinopyroxenes are partly re-equilibrated. In both cases this information is provided by Type-II inclusions, which indicates that the host minerals were already crystallized. The ascent of the carrier magma was continuous and relatively fast, as indicated by the lack of late stage trapping events and by the partial degree of re-equilibration of the inclusions.

The magmas erupted from the Cfz are more differentiated and the distribution of inclusions population is polymodal (Fig. 6). The densest inclusion in an olivine brings to 754 kg·m^{-3} which corresponds to a pressure of 484 MPa. Further trapping of Type-I inclusions with a maximum density of 692 kg·m^{-3} and 497 kg·m^{-3} occurred respectively at 406 MPa and 209 MPa. Accordingly, the degree of re-equilibration of these inclusions is rather high, and many of them did not survived to the multiple ponding.

Finally, the magmas erupted from the SEfz show a similar evolutionary degree to the SERfz, but experienced a non-isochoric ascent, which caused partial re-equilibration in most of the samples. The densest Type-I inclusion (765 kg·m^{-3}) was trapped at 498 MPa, which is quite similar to the value recorded by inclusions from the Cfz. Only a single olivine crystal had a second Type-I fluid trapping event (497 kg·m^{-3}) at 219 MPa.

Magma ponding depths

The assumption that magmas ascend through the lithosphere, stop and accumulate at the Moho Transition Zone (i.e. Stolper and Walker 1980; Bureau et al 1999; Fodor and Galar 1997; Klügel et al. 2005, 2007; Stroncik et al 2009; Hansteen et al 1998; Geist et al 1998; Zanon and Frezzotti 2013) is essential for our calculation of the ponding depth, represented in Figure 11. A country rock density of 2800 kg·m^{-3} was used for the crustal rocks beneath the Serreta submarine ridge, resulting from the direct measurement of our sample, and considered as representative for the crust. This value is in agreement with the measurements performed on lavas from fissure zones in Pico, Faial and São Miguel islands (Zanon and Frezzotti 2013; Zanon 2014). A value of 2500 kg·m^{-3} was used for the crust including the rocks of the island, according to literature (Montesinos et al. 2003; Self 1976) and to the average of three direct density measurements. The deepest level of magma ponding is common to all fissure zone segments and is located between 20.3 and 21 km deep, similarly to the depths reported for Pico and Faial fissure zones (Zanon and Frezzotti, 2013) and is interpreted to represent the Moho Transition Zone.

The magmas of the Cfz show a multi-step ascent with a first crustal ponding depth of 16.5 km, common to all magmas, followed by at least one local ponding 8.5 km deep. At the first ponding site, magmas evolve towards trachybasalt and re-equilibrate the previously trapped fluid inclusions. A new generation of Mg-poor olivines, hosting Type-I fluid inclusions, records this process. The shallower local ponding level is associated to a final step of evolution, characterized by higher degree of fractional crystallization, as revealed by the geochemical characteristics of sample TRS07.

Finally, most magmas of the SEfz ascended without ponding into the crust. Only the magma of a single eruption ponded at 8.9 km deep, however, this stop must have been short, as the evolution degree of the magma is perfectly comparable with that of the other magmas of this segment.

STRESS FIELD OR/AND OCCURRENCE OF DENSITY FILTERS

The petrological characteristics and the microthermometry of fluid inclusions of magmas erupted from the three fissure zone segments reveal slightly different ponding and ascent conditions through the crust. According to our interpretation, these differences were caused by two factors possibly related to one another: the local variation of the stress field and the presence of density barriers that hamper magma ascent.

The Moho Transition Zone is the most efficient barrier, which filters all primitive magmas, promoting fractional crystallization of mantle olivine and pyroxene in rising sub-lithospheric mafic magmas and underplating (e.g. Caress et al. 1995; Charvis et al. 2005; Klügel et al. 2005; Schwarz et al. 2004). At oceanic islands, such as the Azores, it generally corresponds to the transition from ultramafic cumulitic dunites, harzburgites and clinopyroxenites (density ≅3200 $kg{\cdot}m^{-3}$) to partly serpentinized basaltic rocks and/or gabbros with density <2800 $kg{\cdot}m^{-3}$ (e.g. Neumann et al. 1999; Clague and Bohrson 1991; Gaffney 2002).

The orientation of the SEfz is NW-SE, almost orthogonal to the WSW-ENE spreading direction of the Terceira Rift (Marques et al. 2013), i.e. σ_2 and $\sigma_3 \gg \sigma_1$, enabling magma ascent. However, this segment is also influenced by older feeding system of the extinct Cinco Picos central volcano, which hampered the ascent of magma, causing the general re-equilibration of the inclusions.

The Cfz of the island, active in historical times, seems to be dominated by a stress field with a WNW-ESE direction. Due to its position and orientation, the Cfz represents an area of stress transfer from Santa Barbara central volcano, interested by a WNW-ESE tectonic system, to the central volcanoes of Pico Alto and Guilherme Moniz. The ascent of magmas is here both hampered by the direction of the spreading and the presence of intracrustal crystallized bodies of more evolved compositions from the central volcanoes. We interpreted that the latter acted as a density barrier and their presence beneath silicic volcanoes even influenced the local stress field, hampering the propagation of the fissure zone. The presence of density filters beneath Terceira has been previously discussed as a factor that may contribute to the marked bimodal volcanism of the island (e.g. Self and Gunn 1976).

Finally, the SERfz shows a WNW-ESE trend, but the crust here is thought to be free from the presence of pre-existing storage areas of evolved composition. For this reason magmas can ascend rapidly without significant obstacles.

ACKNOWLEDGEMENTS

This study was funded by the Fundação para a Ciência e Tecnologia (PLUSYS project PTDC/CTE-GIX/098836/2008) and VZ was supported by the Fundo Regional para a Ciência, grant 03.1.7.2007.1 (PROEMPREGO Operational Program and Regional Government of the Azores). The authors wish to express their gratitude to Ana Rita Mendes (CVARG, Portugal) for her dedication and patience during the preparation of doubly-polished crystals and to Céline Vidal (IPGP, France) for her fruitful discussion on the statistical management of data. We also thank Stephen Self for the English review. Finally, Steele MacInnis, Andreas Klügel, James Mungall and the editor Rosario Esposito are acknowledged for the significant improvement of this manuscript.

REFERENCES

Andersen, T. and Neumann, E.R. (2001) Fluid inclusions in mantle xenoliths. Lithos, 55(1-4), 301-320.

Bakker, R.J. (2003) Package FLUIDS 1. Computer programs for analysis of fluid inclusion data and for modelling bulk fluid properties. Chemical Geology 194(1), 3-23.

Beattie, P. (1993) Olivine-melt and orthopyroxene-melt equilibria. Contributions to Mineralogy and Petrology, 115(1), 103-111.

Beier, C., Haase, K.M. and Hansteen, T.H. (2006) Magma evolution of the Sete Cidades volcano, São Miguel, Azores. Journal of Petrology, 47, 1375-1411.

Beier, C., Stracke, A. and Haase, K.M. (2007) The peculiar geochemical signatures of São Miguel (Azores) lavas: Metasomatised or recycled mantle sources? Earth and Planetary Science Letters, 259 (1-2), 186-199.

Beier, C., Haase, K.M., Abouchami, W., Krienitz, M.-S. and Hauff, F. (2008) Magma genesis by rifting of oceanic lithosphere above anomalous mantle: Terceira Rift, Azores. Geochemistry, Geophysics, Geosystems, 9(12), Q12013.

Beier, C., Haase, K.M. and Turner, S.P. (2012) Conditions of melting beneath the Azores. Lithos, 144-145, 1-11.

Bodnar, R.J. (2003) Reequilibration of fluid inclusions. In I. Samson, A. Anderson, and D. Marshall, Eds. Fluid Inclusions: Analysis and Interpretation., 32, p. 213-230. Mineral. Assoc. Canada, Short Course.

Bonelli, R., Frezzotti, M.L., Peccerillo, A. and Zanon, V. (2004) Evolution of the volcanic plumbing system of Alicudi (Aeolian Islands): evidence from fluid inclusions in quartz xenoliths. Annals Geophysics, 47(4), 1409-1422.

Bureau, H., Métrich, N., Semet, M.P. and Staudacher, T. (1999) Fluid-magma decoupling in a hot-spot volcano. Geophysical Research Letters, 26(23), 3501-3504.

Calvert, A.T., Moore, R.B., McGeehin, J.P. and Rodrigues da Silva, A.M. (2006) Volcanic history and $^{40}Ar/^{39}Ar$ and ^{14}C geochronology of Terceira Island, Azores, Portugal. Journal of Volcanology and Geothermal Research, 156(1-2), 103-115.

Caress, D.W., McNutt, M.K., Detrick, R.S. and Mutter, J.C. (1995) Seismic imaging of hotspot-related crustal underplating beneath the Marquesas Islands. Nature, 373, 600–603.

Charvis, P., Laesanpura, A., Gallart, J., Hirn, A., Lépine, J.C., de Voogd, B., Minshull, T.A., Hello, Y. and Pontoise, B. (2005) Spatial distribution of hotspot material added to the lithosphere under La Réunion, from wide-angle seismic data. Journal of Geophysical Research, 104, 2875–2893.

Clague, D.A. and Bohrson, W.A. (1991) Origin of xenoliths in the trachyte at Puu Waawaa, Hualalai Volcano, Hawaii. Contributions to Mineralogy and Petrology, 108, 439–452.

Di Martino, C., Frezzotti, M.L., Lucchi, F., Peccerillo, A., Tranne, C. and Diamond, L. (2010) Magma storage and ascent at Lipari Island (Aeolian archipelago, Southern Italy) at 223–81 ka: the role of crustal processes and tectonic influence. Bulletin of Volcanology, 72(9), 1061-1076.

Dixon, J.E. (1997) Degassing of alkalic basalts. American Mineralogist, 82, 368–378.

Dixon, J.E. and Stolper, E.M. (1995) An experimental study of water and carbon dioxide solubilities in Mid-Ocean Ridge basaltic liquids. Part II: applications to degassing. Journal of Petrology, 36(6), 1633-1646.

Fodor, R.V. and Galar, P. (1997) A view into the subsurface of Mauna Kea volcano, Hawaii: crystallization processes interpreted through the petrology and petrography of gabbroic and ultramafic xenoliths. Journal of Petrology, 38(5), 581-624.

Frezzotti, M.L., Andersen, T., Neumann, E.-R. and Simonsen, S.L. (2002) Carbonatite melt–CO_2 fluid inclusions in mantle xenoliths from Tenerife, Canary Islands: a story of trapping, immiscibility and fluid–rock interaction in the upper mantle. Lithos, 64(3), 77-96.

Gaetani, G.A., O'Leary, J.A., N., S., Bulcholz, C.E. and Newville, M. (2012) Rapid re-equilibration of H_2O and oxygen fugacity in olivine hosted melt inclusions. Geology, 40, 915-918.

Gaffney, A. (2002) Environments of crystallization and compositional diversity of Mauna Loa xenoliths, Journal of Petrology, 43, 963– 980.

Galipp, K., Klügel, A. and Hansteen, T.H. (2006) Changing depths of magma fractionation and stagnation during the evolution of an oceanic island volcano: La Palma (Canary Islands). Journal of Volcanology and Geothermal Research, 155(3-4), 285-306.

Geist, D., Naumann, T., and Larson, P. (1998) Evolution of Galápagos Magmas: Mantle and Crustal Fractionation without Assimilation. Journal of Petrology, 39(5), 953-971.

Gertisser, R., Self, S., Gaspar, J.L., Kelley, S.P., Pimentel, A., Eikenberg, J., Barry, T.L., Pacheco, J.M., Queiroz, G. and Vespa, M. (2010) Ignimbrite stratigraphy and chronology on Terceira Island, Azores. In G. Groppelli and L. Viereck-Goette, Eds. Stratigraphy and Geology of Volcanic Areas. Special Paper, 464, p. 133-154. Geological Society of America.

Haase, K.M. and Beier, C. (2003) Tectonic control of ocean island basalt sources on São Miguel, Azores? Geophysical Research Letters, 30, 1856.

Hansteen, T.H., Andersen, T.B., Neumann, E.-R. and Jelsma, H. (1991) Fluid and silicate glass inclusions in ultramafic and mafic xenoliths from Hierro, Canary Islands: Implications for mantle metasomatism. Contributions to Mineralogy and Petrology, 107, 242-254.

Hansteen, T.H. and Klügel, A. (2008) Fluid inclusion thermobarometry as a tracer for magmatic processes. In K. Putirka and F. Tepley, Eds. Reviews in Mineralogy and Geochemistry, 69. Mineralogical Society of America.

Hansteen, T.H., Klügel, A. and Schmincke, H.-U. (1998) Multi-stage magma ascent beneath the Canary Islands: evidence from fluid inclusions. Contributions to Mineralogy and Petrology, 132, 48-64.

Hildenbrand, A., Madureira, P., Ornelas Marques, F., Cruz, I., Henry, B. and Silva, P. (2008) Multi-stage evolution of a sub-aerial volcanic ridge over the last 1.3 Myr: S. Jorge Island, Azores Triple Junction. Earth and Planetary Science Letters, 273(3-4), 289-298.

Klügel, A., Hansteen, T.H. and Galipp, K. (2005) Magma storage and underplating beneath Cumbre Vieja volcano, La Palma (Canary Islands). Earth and Planetary Science Letters, 236, 211-226.

Klügel, A., Hansteen, T.H. and Schmincke, H.-U. (1997) Rates of magma ascent and depths of magma reservoirs beneath La Palma (Canary Islands). Terra Nova, 9(3), 117-121.

Kueppers, U., Nichols, A.R.L., Zanon, V., Potuzak, M. and Pacheco, J.M.R. (2012) Lava balloons - Peculiar products of basaltic submarine eruptions. Bulletin of Volcanology, 74(6), 1379-1393.

Lamadrid, H.M., Lamb, W.M., Santosh, M. and Bodnar, R.J. (2014) Raman spectroscopic characterization of H_2O in CO_2-rich fluid inclusions in granulite facies metamorphic rocks. Gondwana Research, 26, 301-310.

Madureira, P., Mata, J., Mattielli, N., Queiroz, G. and Silva, P. (2011) Mantle source heterogeneity, magma generation and magmatic evolution at Terceira Island (Azores archipelago): Constraints from elemental and isotopic (Sr, Nd, Hf, and Pb) data. Lithos, 126(3-4), 402-418.

Marques, F.O., Catalão, J.C., DeMets, C., Costa, A.C.G. and Hildenbrand, A. (2013) GPS and tectonic evidence for a diffuse plate boundary at the Azores Triple Junction. Earth and Planetary Science Letters, 381, 177-187.

McDonough, W.F. and Sun, S.S. (1995) The composition of the Earth. Chemical Geology, 120(3-4), 223-253.

Miranda, J.M., Mendes Victor, L.A., Simões, J.Z., Luis, J.F., Matias, L., Shimamura, H., Shiobara, H., Nemoto, H., Mochizuki, H., Hirn, A. and Lépine, J.C. (1998) Tectonic setting of the Azores plateau deduced from a OBS survey. Marine Geophysical Researches, 20, 171-182.

Montesinos, F.G., Camacho, A.G., Nunes, J.C., Oliveira, C.S. and Vieira, R. (2003) A 3-D gravity model for a volcanic crater in Terceira Island (Azores). Geophysical Journal International, 154(2), 393-406.

Mungall, J.E. and Martin, R.F. (1995) Petrogenesis of basalt-comendite and basalt-pantellerite suites, Terceira, Azores, and some implications for the origin of ocean-island rhyolites. Contributions to Mineralogy and Petrology, 119(1), 43-55.

Neumann, E.R., Wulff-Pedersen, E., Simonsen, S.L., Pearson, N.J., Martí, J. and Mitjavila, J. (1999) Evidence for fractional crystallization of periodically refilled magma chambers in Tenerife, Canary Islands. Journal of Petrology, 40, 1089–1123.

Putirka, K. (2008) Thermometers and barometers for volcanic systems. In K. Putirka and F. Tepley, Eds. Minerals, inclusions and volcanic processes, Reviews in Mineralogy and Geochemistry, 69, p. 61-120. Mineralogical Society of America.

Quartau, R., Hipólito, A., Romagnoli, C., Casalbore, D., Madeira, J., Tempera, F., Roque, C. and Chiocci, F.L. (2014) The morphology of insular shelves as a key for understanding the geological evolution of volcanic islands: Insights from Terceira Island (Azores). Geochemistry, Geophysics, Geosystems, 15(5), 1801–1826.

Roedder, E. (1965) Liquid CO_2 inclusions in olivine-bearing nodules and phenocrysts from basalts. American Mineralogist, 50, 1746-1782.

Roedder, E. (1983) Geobarometry of ultramafic xenoliths from Loihi Seamount, Hawaii, on the basis of CO_2 inclusions in olivine. Earth and Planetary Science Letters, 66, 369-379.

Schwarz, S., Klügel, A. and Wohlgemuth-Ueberwasser, C. (2004) Melt extraction pathways and stagnation depths beneath the Madeira and Desertas rift zones (NE Atlantic) inferred from barometric studies. Contributions to Mineralogy and Petrology, 147(2), 228-240.

Self, S. (1976) The recent volcanology of Terceira, Azores. Journal of the Geological Society of London, 132, 645-666.

Self, S. and Gunn, B.M. (1976) Petrology, volume, and age relations of alkaline and saturated peralkaline volcanics from Terceira, Azores. Contributions to Mineralogy and Petrology, 54, 293-313.

Shejwalkar, A. and Coogan, L.A. (2013) Experimental calibration of the roles of temperature and composition in the Ca-in-olivine geothermometer at 0.1 MPa. Lithos, 177(0), 54-60.

Silveira, G., Vinnik, L., Stutzmann, E., Farra, V., Kiselev, S. and Morais, I. (2010) Stratification of the Earth beneath the Azores from P and S receiver functions. Earth and Planetary Science Letters, 299, 91-103.

Span, R. and Wagner, W. (1996) A new equation of state for carbon dioxide covering the fluid region from the triple point temperature to 1100 K at pressures up to 800 MPa. Journal of Physical and Chemical Reference Data, 25, 1509-1596.

Sterner, S.M. and Bodnar, R.J. (1991) Synthetic fluid inclusions; X, Experimental determination of P-V-T-X properties in the CO_2 -H_2O system to 6 kb and 700 degrees C. American Journal of Science, 291(1), 1-54.

Sterner, S.M. and Pitzer, K.S. (1994) An equation of state for carbon dioxide valid from zero to extreme pressures. Contributions to Mineralogy and Petrology, 117, 362-374.

Stolper, E. and Walker, D. (1980) Melt density and the average composition of basalt. Contributions to Mineralogy and Petrology, 74(1), 7-12.

Stroncik, N.A., Klügel, A. and Hansteen, T.H. (2009) The magmatic plumbing system beneath El Hierro (Canary Islands): constraints from phenocrysts and naturally quenched basaltic glasses in submarine rocks. Contributions to Mineralogy and Petrology, 157(5), 593-607.

Sun, S.S. and McDonough, W.F. (1989) Chemical and isotopic systematics of ocean basalts: implications for mantle composition and processes. In A.D. Saunders and M.J. Norry, Eds. Magmatism in ocean basin. 42, p. 313-345. Geol. Soc. London. Spec. Pub.

Tzanis, A. and Makropoulos, K. (1999) Magnetotellurics and seismotectonics in the analysis of active domains: An essential combination? Physics and Chemistry of the Earth, Part A: Solid Earth and Geodesy, 24(9), 841-847.

Viti, C. and Frezzotti, M.-L. (2000) Re-equilibration of glass and CO_2 inclusions in xenolith olivine: A TEM study. American Mineralogist, 85(10), 1390-1396.

-. (2001) Transmission electron microscopy applied to fluid inclusion investigations. Lithos, 55(1-4), 125-138.

Zanon, V. and Frezzotti, M.L. (2013) Magma storage and ascent conditions beneath Pico and Faial islands (Azores Islands). A study on fluid inclusions. Geochemistry, Geophysics, Geosystems, 14(9), 3494–3514.

Zanon, V., Frezzotti, M.L. and Peccerillo, A. (2003) Magmatic feeding system and crustal magma accumulation beneath Vulcano Island (Italy): evidence from fluid inclusions in quartz xenoliths. Journal of Geophysical Research, 108(B6), 2298-2310.

Zanon, V., Kueppers, U., Pacheco, J.M. and Cruz, I. (2013) Volcanism from fissure zones and the Caldeira central volcano of Faial Island, Azores archipelago: geochemical processes in multiple feeding systems. Geological Magazine, 130(3), 536-555.

Zanon, V. and Nikogosian, I. (2004) Evidence of crustal melting events below the Island of Salina (Aeolian Arc, Southern Italy). Geological Magazine, 141(4), 525-540.

Zanon, V. (2014) Conditions for mafic magma storage beneath fissure zones at oceanic islands. The case of São Miguel island (Azores archipelago). Journal of the Geological Society of London, in press.

Figure Captions

FIGURE 1. a) Geographic sketch map of the Azores archipelago showing main structural features as dashed lines. MAR: Mid-Atlantic Ridge; TR: Terceira Rift; EAFZ: East Azores Fracture Zone; GF: Gloria Fault. Blue circle marks location of Terceira Island. b) Digital elevation model of Terceira showing axes of fissure zone segments, main volcanic and tectonic features and vents of historical eruptions (basaltic magmas). Stars locate sample sites and grey arrows indicate main paths of lava flows interpreted from aerophotographs. Cfz: Central fissure zone segment; SEfz: Southeastern fissure zone segment; SERfz: Serreta submarine fissure zone segment. UTM coordinates in km.

FIGURE 2. Temporal sequence of eruption of the lavas from different segments of the fissure zone. Sample numbers indicated in red. Coordinates correspond, whenever possible, to the source vent of the samples, measured as easting (UTM coordinates in km). Age correlations from Self (1976), updated with Calvert et al. (2006). The thick dashed line represents the Lajes-Angra Ignimbrite formation temporal marker (~21 ka). Fissure zone acronyms as in Fig. 1.

FIGURE 3. Photomicrographs of selected basaltic samples from Terceira. a) Poorly porphyritic lavas of the Cfz (TRS01) showing few microphenocryts of plagioclase and rare mafic phases dispersed in a crystalline groundmass of feldspars, olivines, clinopyroxenes and oxides (not visible). b) Porphyritic basalt of the SEfz (TRS06) showing the occurrence of phenocrysts (0.8-0.5 mm) and microphenocrysts (~0.3 mm) of olivine and a basal section of a clinopyroxene. c) Coexistence of scattered Type-I with short trails of Type-II fluid inclusions and silicate melt inclusions (MIs).

FIGURE 4. a) Total Alkali Silica (TAS) classification diagram of the samples shows limited variability of composition. Porphyritic samples of the SEfz are basalt, while those crystal-poor of the Cfz are trachybasalt and basalt. b) Primordial-mantle-normalized patterns of incompatible elements (McDonough and Sun 1995) are all very similar, despite the degree of evolution of the samples. The lava balloons sample of the AD 1998-2001 eruption is among the least evolved, while the lavas of the Cfz are the most evolved. c) The chondrite-normalized patterns of Rare Earth Elements (Sun and McDonough 1989) confirm this observation. No negative Eu anomaly is observed in the studied samples.

FIGURE 5. a) Possible compositional evolution path by fractional crystallization of mafic phases and plagioclase. Each vector qualitatively indicates the direction of the compositional array in the case of single phase removal. b) Ratios among LILE (e.g. Rb/Ba) and U/Th are variable and beyond the analytical error, indicating that this chemical heterogeneity is inherited by the mantle source. A suite of rocks produced by the removal of mafic phases from the same parental liquid should preserve these ratios. d) Variations of the ratios among LREE/HREE in basaltic compositions are also too large to be explained by clinopyroxene and olivine fractionation.

FIGURE 6. a) Histograms of Th_L of fluid inclusions in olivines and clinopyroxenes. The data are polymodal and representative of the three fissure zone segments. Data population from the lava balloons sample is large, while that from the poorly porphyritic samples of the Cfz is small. The few data of Th_V are not reported here for convenience. b) Histograms of the total density values of the trapped fluid, divided in the same classes as for the temperatures of the homogenization. These histograms also include the few density data of the inclusions which homogenized into the vapor.

FIGURE 7. Relation between the size of the inclusions and their temperature of homogenization. Four small trails of inclusions in a single olivine show that the lowest Th_L characterizes the smallest inclusion in each trail. The increase in Th_L is directly related to the size, due to re-equilibration processes.

FIGURE 8. Diagram of the crystallization temperatures calculated from the application of Ca-in olivine geothermometer (Shejwalkar and Coogan 2013) to the composition of phenocrysts and microphenocrysts from three samples. The vertical bar represents the maximum error observed

for this algorithm (±20 °C). The data also include compositions of olivine phenocrysts from the lava balloons of the AD 1998-2001 submarine eruption (Kueppers et al. 2012).

FIGURE 9. Isochores for selected samples of fissure zone segments. The lines related to pure CO_2 fluid derived from the application of the equation of Span and Wagner (1996) and are represented by grey dashed lines. Those for H_2O+CO_2 (molar ratio 1:9) fluids, represented by light-blue dashed lines, are obtained from the equation of Sterner and Bodnar (1991). The yellow vertical line is the intercepts of isochores with calculated temperature of trapping of the fluids.

FIGURE 10. Pressures scheme of trapping events and re-equilibration for the studied samples. Green and red colors discriminate information from inclusions trapped in clinopyroxenes and olivines, respectively. Arrows indicate re-equilibrated populations of inclusions. The black dashed line marks the limit between the pure fissure zone domain of the Serreta submarine ridge from the subaerial fissure zone segments passing through pre-existing storage systems.

FIGURE 11. Scheme of the distribution of magma storage systems of fissure zone segments across an ideal NW-SE profile of Terceira Island. The areas of fluid trapping are indicated by the pattern and by the thin blue dashed lines. The two thick blue dashed lines represent the possible location of the Moho Transition Zone. For further explications, please refer to the text.

Table list

TABLE 1. Brief description of the samples, representative of the different segments of the fissure zone. Unit names and ages from Self (1976) updated with Calvert et al. (2006). Phenocrysts and microphenocrysts are counted together in modal data.

TABLE 2. Summary of fluid inclusions data. Data report the range measured. Density values are re-calculated in consideration of a composition of the fluid of H_2O+CO_2 with a molar ratio of 1:9.

Supplementary material

Supplementary datatable1 - Chemical database of whole-rock compositions.

Supplementary datatable2 - Microprobe analyses of the mineral assemblage of selected samples and the groundmass glass. Mineral chemistry comes from the core of the crystals, using a spot beam. Groundmass glasses were analyzed with a defocalized beam. Most of the data are from single spot, except the trimmed mean (15% of extreme data) of 14 analyses. In this latter case, the standard deviation is reported in parentheses.

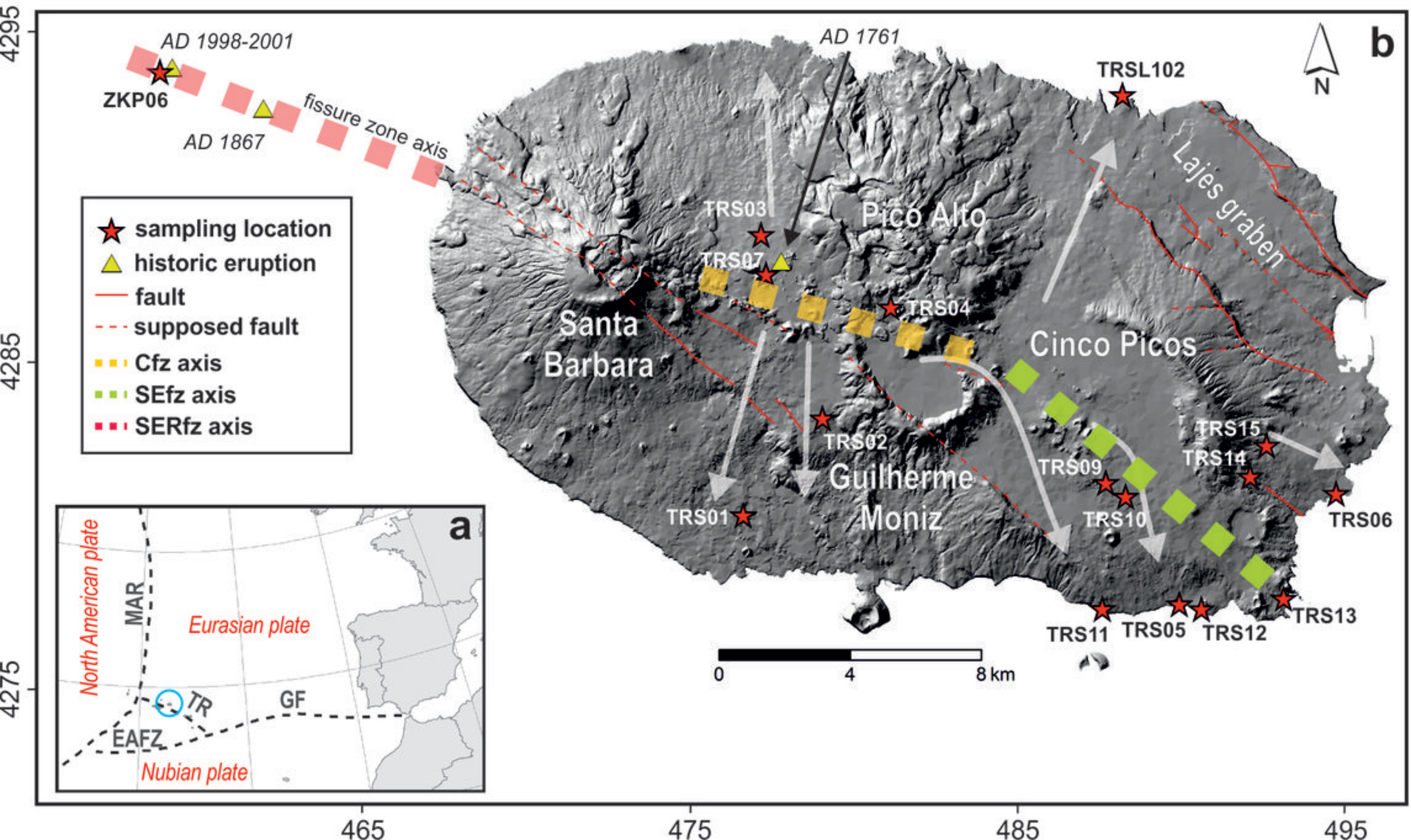

b
a
AD 1998-2001
AD 1761
AD 1867
ZKP06
fissure zone axis
TRSL102
N
Pico Alto
Lajes graben
sampling location
historic eruption
fault
supposed fault
Cfz axis
SEfz axis
SERfz axis
TRS03
TRS07
TRS04
TRS02
TRS01
TRS09
TRS10
TRS14
TRS15
TRS06
TRS11
TRS05
TRS12
TRS13
Santa
Barbara
Cinco Picos
Guilherme
Moniz
0
4
8 km
North American plate
Eurasian plate
Nubian plate
MAR
TR
GF
EAFZ
4295
4285
4275
465
475
485
495

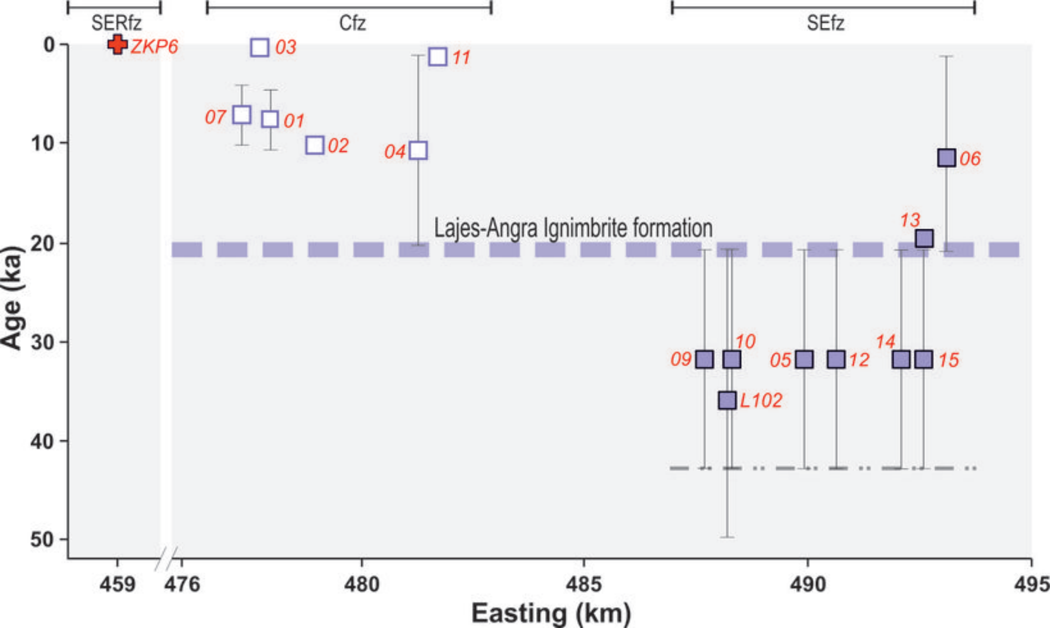
SERfz
Cfz
SEfz
ZKP6
03
11
07
01
02
04
06
13
Lajes-Angra Ignimbrite formation
09
10
L102
05
12
14
15
Age (ka)
0
10
20
30
40
50
459
476
480
485
490
495
Easting (km)

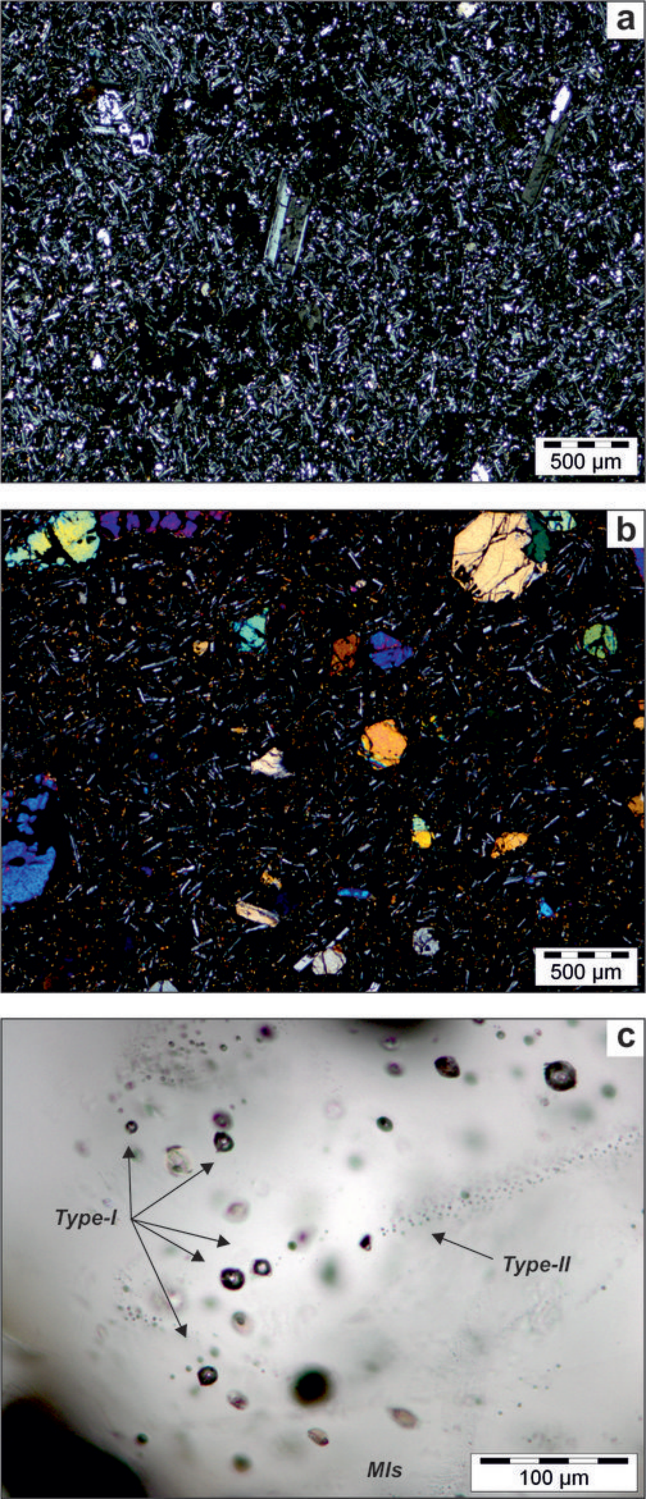
a
500 µm
b
500 µm
c
Type-I
Type-II
MIs
100 µm

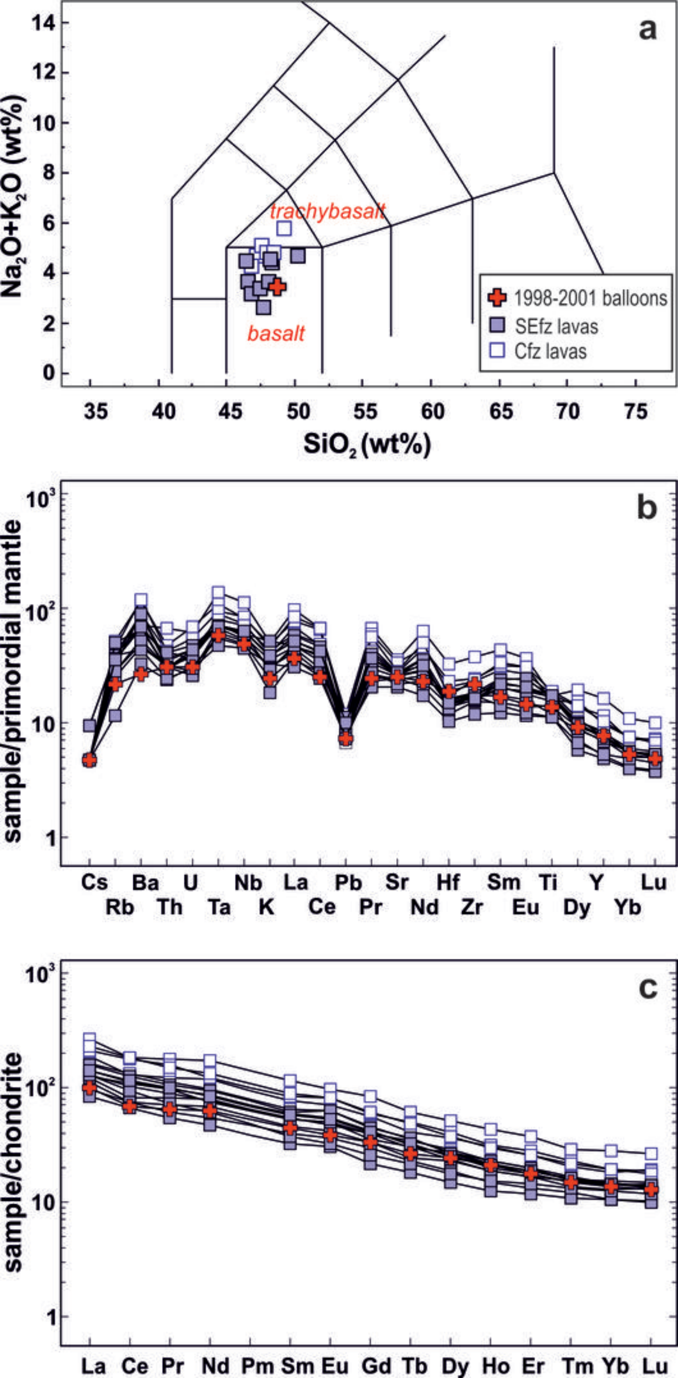
a
b
c
trachybasalt
basalt
1998-2001 balloons
SEfz lavas
Cfz lavas
Na_2O+K_2O (wt%)
SiO_2 (wt%)
sample/primordial mantle
sample/chondrite
Cs Rb Ba Th U Ta Nb K La Ce Pb Pr Sr Nd Hf Zr Sm Eu Ti Dy Y Yb Lu
La Ce Pr Nd Pm Sm Eu Gd Tb Dy Ho Er Tm Yb Lu

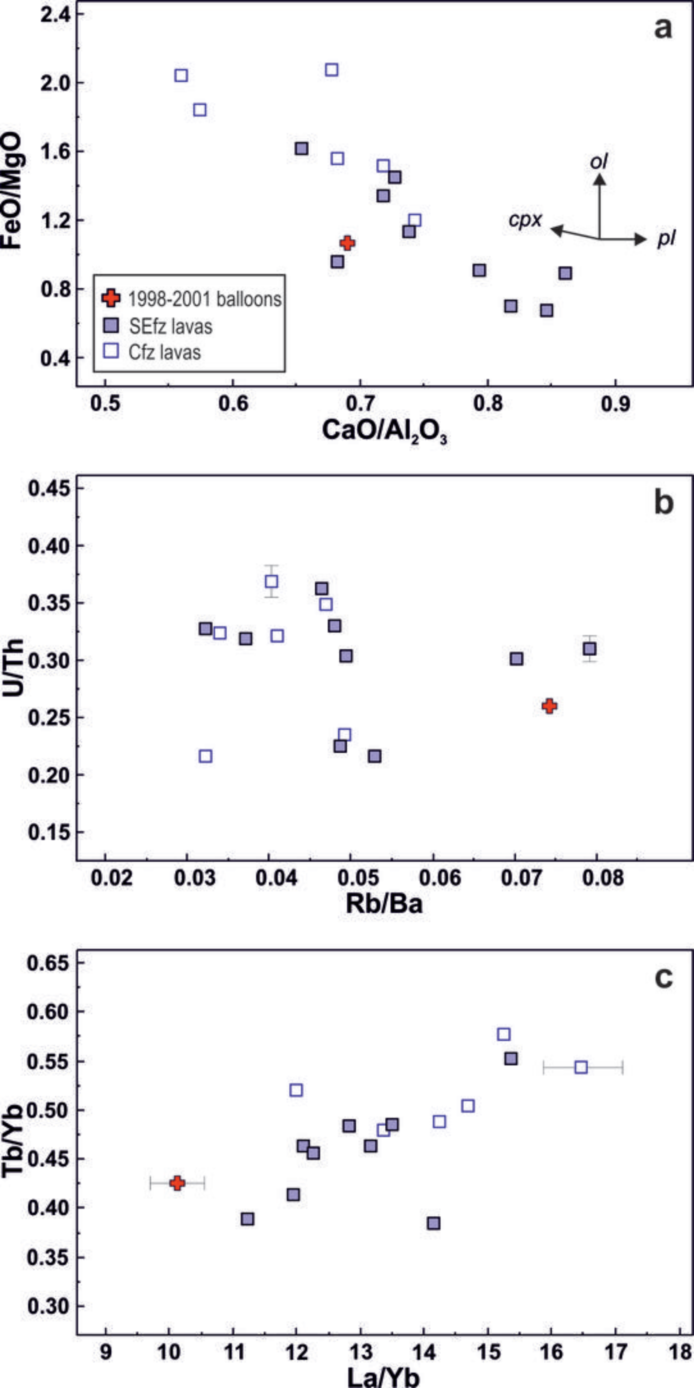
a
b
c
FeO/MgO
CaO/Al_2O_3
U/Th
Rb/Ba
Tb/Yb
La/Yb
ol
cpx
pl
1998-2001 balloons
SEfz lavas
Cfz lavas

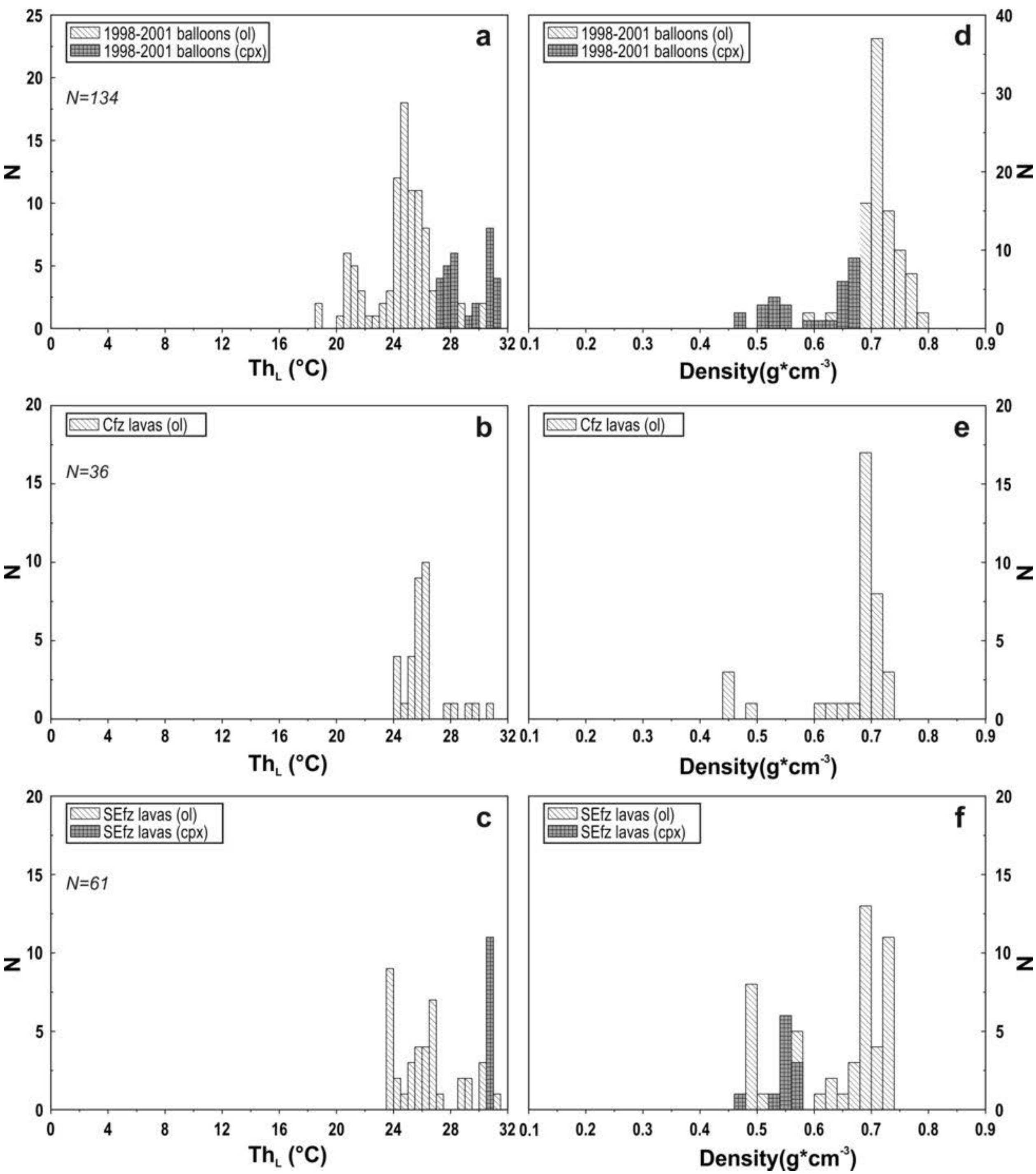

1998-2001 balloons (ol)
1998-2001 balloons (cpx)
a
N=134
N
Th_L (°C)
d
Density(g*cm-3)
Cfz lavas (ol)
b
N=36
e
SEfz lavas (ol)
SEfz lavas (cpx)
c
N=61
f

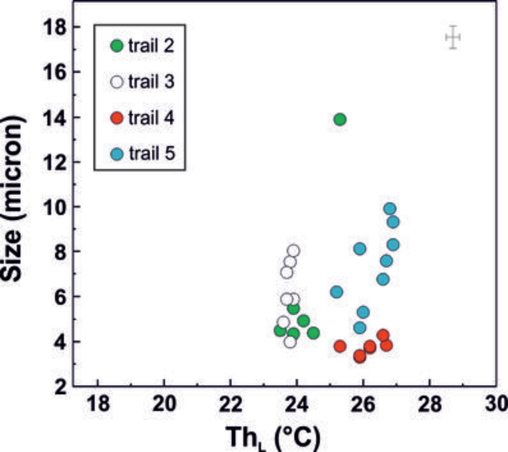

trail 2
trail 3
trail 4
trail 5
Size (micron)
18
16
14
12
10
8
6
4
2
18
20
22
24
26
28
30
Th_L (°C)

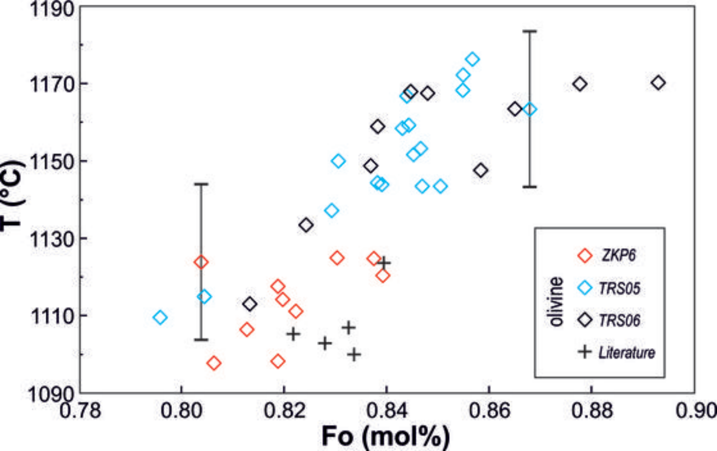

1190
1170
1150
1130
1110
1090
T (°C)
0.78
0.80
0.82
0.84
0.86
0.88
0.90
Fo (mol%)
olivine
ZKP6
TRS05
TRS06
Literature

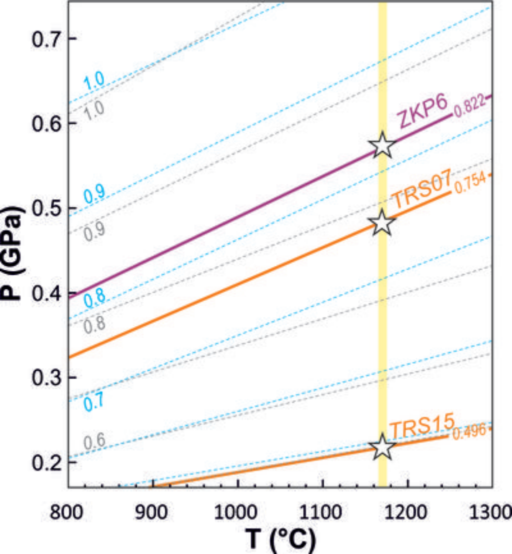

P (GPa)
T (°C)
0.7
0.6
0.5
0.4
0.3
0.2
800
900
1000
1100
1200
1300
1.0
1.0
0.9
0.9
0.8
0.8
0.7
0.6
ZKP6
0.822
TRS07
0.754
TRS15
0.496

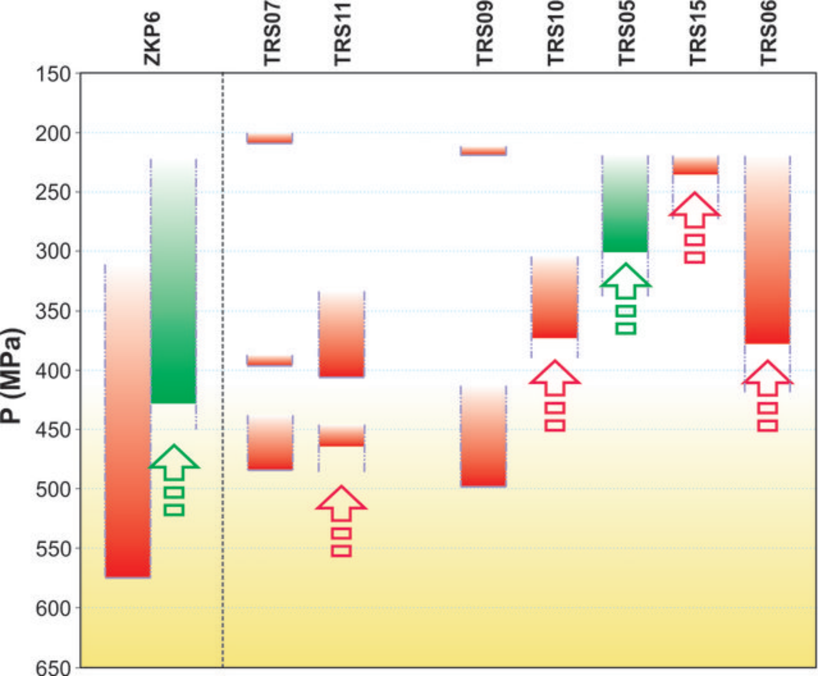

ZKP6
TRS07
TRS11
TRS09
TRS10
TRS05
TRS15
TRS06
P (MPa)
150
200
250
300
350
400
450
500
550
600
650

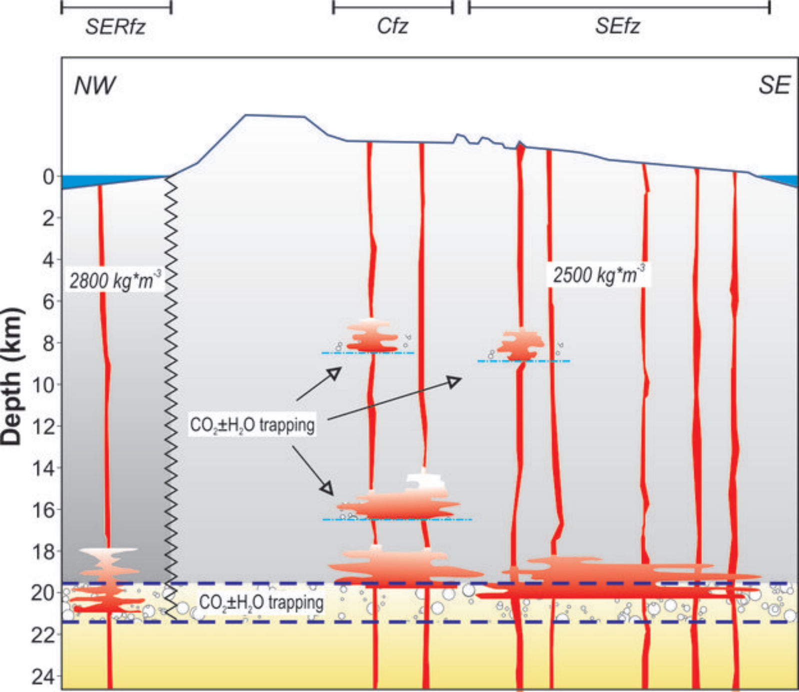

SERfz
Cfz
SEfz
NW
SE
Depth (km)
0
2
4
6
8
10
12
14
16
18
20
22
24
2800 kg*m^{-3}
2500 kg*m^{-3}
$CO_2 \pm H_2O$ trapping
$CO_2 \pm H_2O$ trapping

TABLE 1. Brief description of the samples, representative of different segments of the fissure zone. Unit names and ages from Self (1976) updated with Calvert et al. (2006).

Sample	Easting Northing	Unit/Location	Volcanic System	Age (years BP)	Texture	Modal analysis	Occurrence of fluid inclusions
TRS01	476611 E 4280357 N	Bagacina flow	Cfz	<10,090±50 and >4480±40	intergranular to intersertal	$pl_{16}+ol_{5}+cpx_{2}+ox_{6}+gms_{71}$	not found
TRS02	479036 E 4283318 N	Vareiras flow	Cfz	10,090±50	intersertal	$pl_{18}+ol_{10}+cpx_{5}+ox_{10}+gms_{57}$	not found
TRS03	477159 E 4288907 N	historic flow	Cfz	AD 1761	intersertal with glomeroporphyritic aggregates	$pl_{26}+ol_{3}+cpx_{3}+ox_{14}+gms_{54}$	not found
TRS04	481117 E 4286700 N	unnamed cone	Cfz	>1910±35	intersertal	$ol_{7}+pl_{5}+cpx_{2}+ox_{7}+gms_{79}$	not found
TRS05	489915 E 4277647 N	Porto Judeu	SEfz	>21,000	-	-	cpx
TRS06	494696 E 4281018 N	Porto S. Fernando	SEfz	<21,000	intersertal	$pl_{18}+ol_{16}+cpx_{6}+ox_{6}+gms_{54}$	ol
TRS07	477312 E 4287701 N	Pico 599	Cfz	>4480±40 and <10,090±50	-	-	ol
TRS09	487671 E 4281350 N	base of Cinco Picos caldera	SEfz	>21,000	intersertal with glomeroporphyritic aggregates	$ol_{17}+pl_{15}+cpx_{6}+ox_{3}+gms_{59}$	ol
TRS10	488280 E 4280926 N	base of Cinco Picos caldera	SEfz	>21,000	intersertal to seriate	$pl_{17}+ol_{7}+cpx_{1}+ox_{10}+gms_{65}$	ol
TRS11	487566 E 4277502 N	Algar do Carvão flow	Cfz	1910±35	intergranular to intersertal	$ol_{7}+pl_{2}+cpx_{18}+ox_{11}+gms_{63}$	ol
TRS12	490587 E 4277495 N	Pico do Refugo	SEfz	>21,000	intersertal	$ol_{16}+pl_{3}+cpx_{1}+ox_{4}+gms_{76}$	not found
TRS13	493093 E 4277817 N	near Pico dos Comos	SEfz	19,120±50?	intersertal	$pl_{18}+ol_{7}+cpx_{3}+ox_{7}+gms_{65}$	not found
TRS14	492075 E 4281540 N	Fonte do Bastardo	SEfz	>21,000	intersertal	$ol_{4}+cpx_{3}+pl_{1}+ox_{3}+gms_{89}$	not found
TRS15	492578 E 4282484 N	Fonte do Bastardo	SEfz	>21,000	intersertal	$pl_{14}+ol_{6}+cpx+ox_{4}+gms_{76}$	ol
TRSL102	488179 E 4293179 N	Ponta das Escaleiras	SEfz	>21,000 and <50,000±10,000	intersertal	$pl_{19}+ol_{11}+cpx_{2}+ox_{9}+gms_{59}$	not found
ZKP06	458828 E 4293879 N	~10 km offshore Terceira	SERfz	AD 1998-2001	vitrophyric with cryptocrystals to intersertal	$pl_{24}+ol_{12}+cpx+gms_{64}$	ol+cpx

Mineral modal counting (%) is indicated in subscripts. Acronyms: ol – olivine, pl – plagioclase, cpx – clinopyroxene, ox – oxides (unspecified), gms – groundmass; Cfz - Central fissure zone segment; SEfz - Southeastern fissure zone segment; SERfz - Serreta submarine fissure zone segment.

TABLE 2: Fluid inclusions data

Sample	N° measures	Host	Th_L (°C)	Th_V (°C)	Density ($kg\cdot m^{-3}$)	P (MPa)	Depth (km)
TRS05	11	cpx	30.5-31		496-590	222-301	9.1-12.3
TRS06	11	ol	28.6-31		497-669	219-378	8.9-15.4
TRS07	19	ol	24.3-28.0	31	482-754	209-484	8.5-19.8
TRS09	36	ol	23.5-31		497-765	219-498	8.9-20.3
TRS10	2	ol	28.8-30.4		598-664	303-373	12.4-15.2
TRS11	17	ol	25.2-29.8		629-739	334-464	13.6-18.9
TRS15	1	ol	31		497	219	8.9
ZKP06	30	cpx	27.2-31.0		487-703	222-428	8.1-15.6
ZKP06	104	ol	18.8-30.2		610-822	315-575	11.5-21.0